

# Seeing the faults from the hummocks: tectonic or landslide fault discrimination with LiDAR at Mt Shasta, California

Riccardo Tortini<sup>1\*</sup>, Benjamin van Wyk de Vries<sup>2</sup> and Simon A. Carn<sup>1</sup>

<sup>1</sup> Department of Geological and Mining Engineering and Sciences, Michigan Technological University, Houghton, MI, USA,

<sup>2</sup> Laboratoire Magmas et Volcans, Université Blaise-Pascal - Centre National de la Recherche Scientifique - IRD, OPGC, Clermont-Ferrand, France

## OPEN ACCESS

### Edited by:

Luis E. Lara,  
Servicio Nacional de Geología y  
Minería, Chile

### Reviewed by:

Alessandro Tibaldi,  
University of Milano-Bicocca, Italy  
Alfredo Mahar Francisco Amante  
Lagmay,  
University of the Philippines,  
Philippines  
Felipe Aron,  
Stanford University, USA

### \*Correspondence:

Riccardo Tortini,  
Integrated Remote Sensing Studio,  
University of British Columbia, 2424  
Main Mall, Vancouver, BC V6T1Z4,  
Canada  
riccardo.tortini@ubc.ca

### Specialty section:

This article was submitted to  
Volcanology,  
a section of the journal  
Frontiers in Earth Science

**Received:** 04 February 2015

**Accepted:** 05 August 2015

**Published:** 19 August 2015

### Citation:

Tortini R, van Wyk de Vries B and Carn SA (2015) Seeing the faults from the hummocks: tectonic or landslide fault discrimination with LiDAR at Mt Shasta, California. *Front. Earth Sci.* 3:48. doi: 10.3389/feart.2015.00048

The detection of active faults around volcanoes is of importance for both seismic and volcanic hazard assessment. The lower flanks of volcanoes are, however, often covered by debris avalanche deposits (DADs) that are highly faulted during transport. Such areas are dissected by faults that delineate deposit hummocks, making it hard to differentiate tectonic from landslide structures. Detailed analysis of DAD surface morphology can detect fault trends not compatible with landslide emplacement, but which do follow regional trends or cut hummocks. Indeed, neotectonic faults may also cut across avalanche structure and morphology and thus be distinguishable. We present evidence of neotectonic deformation along a north-south trending fault, cutting across the 300 ka BP Mt Shasta DAD. The fault was identified on an airborne LiDAR campaign and then confirmed in the field. The discovery emphasizes the value of high-resolution topographic mapping of such areas, and exposes a previously unknown fault. In this particular case the identified fault is not long, and may not present a strong seismic hazard to the sparsely populated area, but the full area of the DAD has not been mapped and there are suggestions from lower resolution datasets that other faults may be present outside the LiDAR coverage, indicating that the Shasta basin could be more seismically active than presently thought. We speculate that this may be part of a westward extension of the Klamath basin rifting. Many DADs at the base of other volcanoes are highly populated and fault detection in these zones could have a significant impact on hazard assessment.

**Keywords:** Shasta, volcano, LiDAR, fault, debris avalanche deposit

## Introduction

A large number of stratovolcanoes are at least partially surrounded by broad piedmonts of hummocky landslide materials. Some volcanoes are emplaced on large tectonic faults (e.g., Socompa, Wadge et al., 1995; Iriga, Paguican et al., 2012), while others generate major faults around their base by gravitational and magmatic deformation (e.g., Poas, Borgia et al., 1990; Etna, Acocella and Neri, 2005; Fuji, Matsuda et al., 1978; Merapi, Walter et al., 2007; Mombacho, Shea et al., 2008). Volcanic landslide deposits have the tendency to mask the tectonic deformation. For example, debris avalanche deposits (DADs) are highly faulted during emplacement, and thus they form an obscuring belt that can mask evidence of other faulting. Landslides are often generated

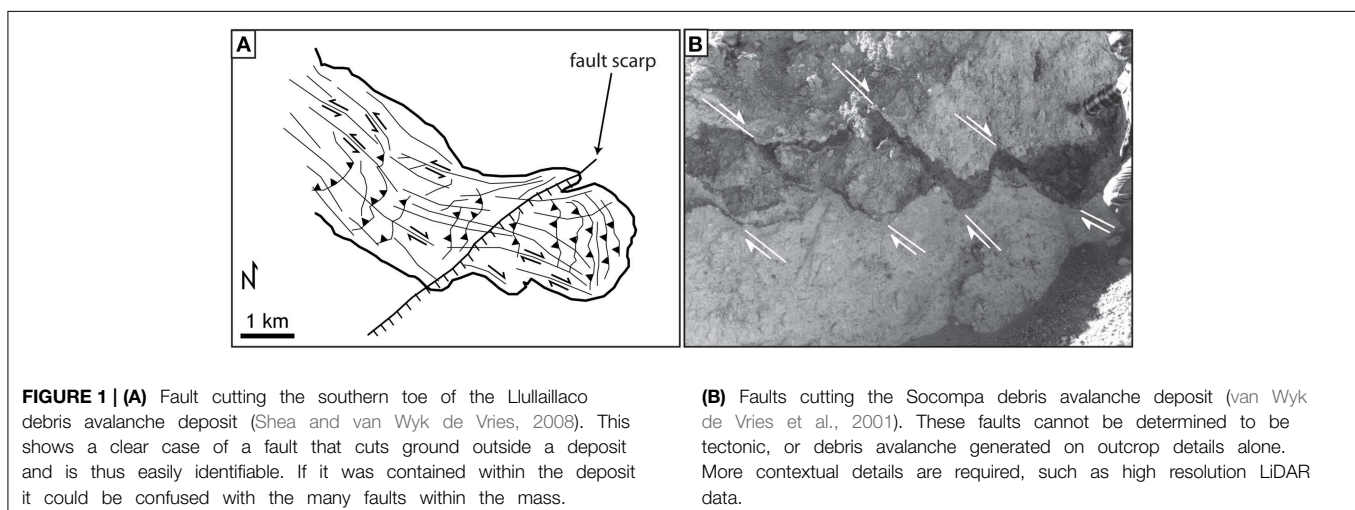
and triggered by faults and the resulting deposits tend to accumulate over these same faults (Wooller et al., 2004). This is a general problem where field examination (such as by seismic stratigraphy—the study of neotectonic faulting in cross sections) may have difficulty separating the two types of deformation, and of detecting important tectonic faulting. The hummocks left in landslides are principally the result of horst and graben extension, strike-slip deformation and fault anticline compression produced within the sliding, spreading mass (Paguican et al., 2012). These structures are identical at outcrop scale to those produced by regional tectonics or local gravitational tectonics, with the exception that they bottom out at the slide base and that their geometry is related to the landslide. Hummocks tend to be unstable, and so may continue to develop their own internal failure even long after the landslide has been emplaced. This may cause neotectonic-like features that may be confused with regional faulting. Examples of this occurrence can be observed at volcanoes worldwide, such as Iriga, Philippines (strike-slip fault on Buhi deposit; Paguican et al., 2012), Mombacho, Nicaragua (possible fault on El Crater deposit; Shea et al., 2008), Llullaillaco, Chile (enigmatic structure on lower lobe; Richards and Villeneuve, 2001), Socompa, Chile (deposit obscured spreading structures; van Wyk de Vries et al., 2001), and on Olympus Mons, Mars (confusion about aureole structures; Morris, 1982; McGovern et al., 2004). The Llullaillaco example (**Figure 1A**) shows a clear case of a fault that extends beyond a deposit and is thus easily identifiable. If it was contained within the deposit it could be confused with the many faults within the mass. However, other faults in other deposits can't be determined to be tectonic or debris avalanche generated on the outcrop details alone (e.g., Socompa, **Figure 1B**). The detection of regional and gravitational tectonics thus requires a special methodology and high-resolution topographic data to detect structural morphology not compatible with landsliding but consistent with large-scale deformation.

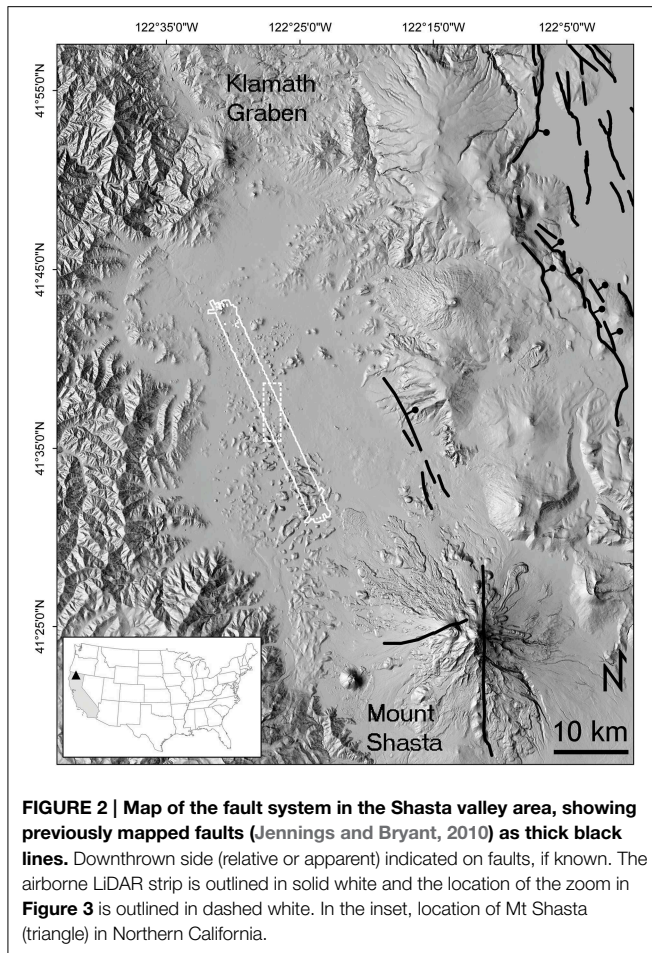
Here, we provide an example of a post-avalanche fault detected with LiDAR on the Mt Shasta (California, USA;

**Figure 2**) landslide, and describe the methodology required to identify it. Mt Shasta is located in the southern part of the Cascade volcanic arc, an extensional magmatic arc extending from Northern California, USA, to British Columbia, Canada. The Cascades formed by the subduction of the Juan de Fuca plate beneath North America (Harper and Wright, 1984; Guffanti and Weaver, 1988; Blakely et al., 1997; Schmidt et al., 2008). These arc volcanoes are located in a segmented series of rifts that extends northwards from the Klamath graben, ~40 km west of Mt Shasta. This graben is at the termination of the Walker Lane, a broad strike-slip lineament forming the eastern boundary of the Sierra Nevada (Faulds et al., 2005) The current Mt Shasta edifice is 4322 m a.s.l. high and has an estimated volume of 350 km<sup>3</sup>, and formed on the remnants of the ancestral Shasta volcano, destroyed by an avalanche ~300,000–380,000 years ago (Crandell et al., 1984). This sector collapse produced one of the largest DADs observable on Earth, reaching a distance of ~40 km from the original volcanic edifice and characterized by hummocky topography and elongated ridges with distinct geometry. Such large-scale collapses are often associated with significant previous gravitational and tectonic deformation (van Wyk de Vries and Davis, 2015), so for Shasta, pre and post-avalanche faulting is expected. The fault we discover is located in a zone where no faults have been mapped to date, and is therefore important for seismic hazard assessment and for volcano-tectonic interactions at Mt Shasta.

## Materials and Methods

Airborne Light Detection and Ranging (LiDAR) systems measure distance by illuminating a target with a laser from a moving platform and analyzing the reflected light. The laser beam is directed toward the ground as the survey aircraft flies over the target area, so that the time between the pulse and the returned reflection can be measured to determine the distance between the instrument and the ground (Petrie and Toth, 2009). Inertial guidance and GPS units track and record the position and





orientation of the airborne platform in time, and the integration of the laser beam travel time, inertial measurement unit (IMU), and GPS determines the position in space of each reflection (Wehr, 2009).

Airborne LiDAR allows for rapid and accurate generation of digital terrain models (DTMs). A DTM is a continuous function that maps from 2D planimetric position to terrain elevation (Pfeifer and Mandlbürger, 2009). Over the past decade DTMs derived from airborne LiDAR surveys have been used to detect and characterize surface faults with known location and primarily in areas with significant geologic structure (e.g., Haugerud et al., 2003; Wieczorek et al., 2004; Egnew, 2005; Hilley and Arrowsmith, 2008; Arrowsmith and Zielke, 2009; Hilley et al., 2010; Zielke et al., 2010; Stumpf et al., 2013), but also in urban areas (Engelkemeir and Khan, 2008; Kondo et al., 2008) and in some cases beneath dense vegetation cover (Harding and Berghoff, 2000; Lin et al., 2013).

The Mt Shasta DAD LiDAR data (DOI: 10.5069/G97P8WB8) were acquired on August 5th, 2013 by the National Center for Airborne Laser Mapping (NCALM) as part of the seed grant ID 2013-08, entitled “A deeper insight into the largest reported Quaternary debris avalanche on Earth: the case of Mount Shasta volcano, northern California” (**Figure 2**). The goal of the project

was to gather high precision topographic data to characterize the distribution of the hummocks in the Shasta deposit.

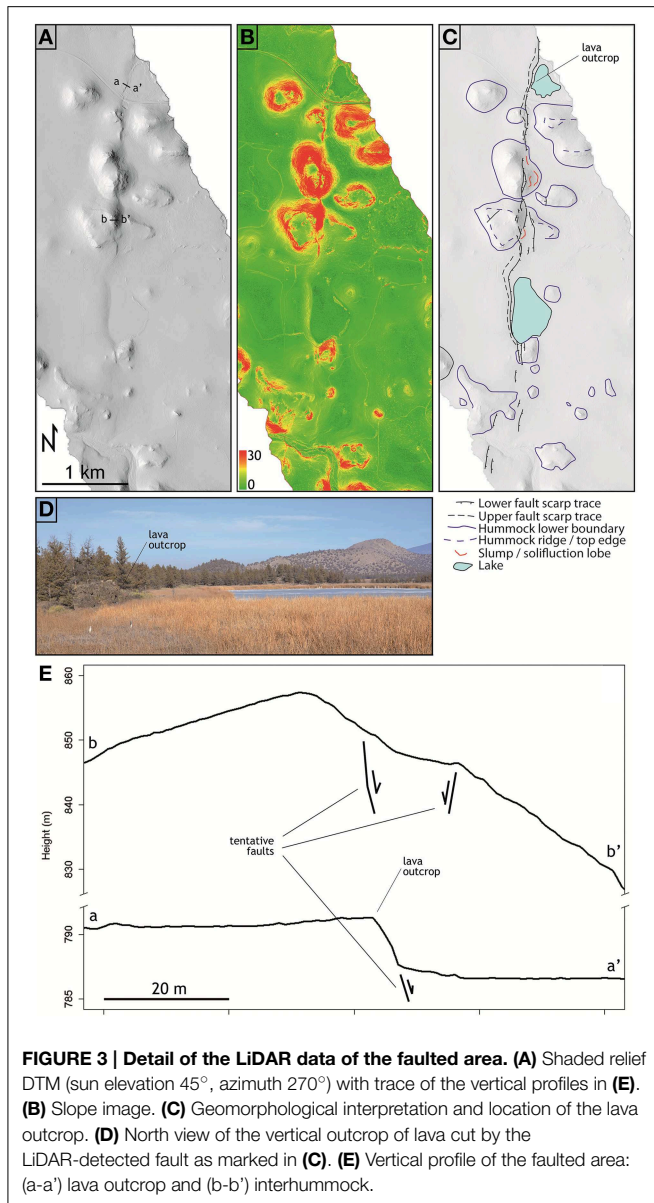
An Optech Airborne Laser Terrain Mapper Gemini was mounted in a Cessna 337 Skymaster and flown at about 600 m above ground level. The scanner was operated at 50 kHz with a 16° scan angle, resulting in a total swath area of 48.57 km<sup>2</sup> and dot spacing (i.e., horizontal resolution) of 1 m. No ground control points were collected for this project, hence, a <0.15 m vertical bias in the elevations of the final point cloud and DEM may exist with respect to NAVD88. The Optech Gemini sensor acquires two returns from a single outgoing laser pulse, which permits penetration of the vegetation canopy. Reflections in the Shasta DAD are returned from the ground, vegetation, roads and buildings. Although not densely vegetated and largely unaffected by human activities, in this work we used the LiDAR second return in order to remove non-ground returns and obtain a bare-earth DTM.

Hillshading is a technique in which the surface of a DTM is illuminated from a particular sun position. Surfaces inclined toward the illumination source are lighter than average, whereas surfaces inclined away are darker (i.e., shadowed). Other techniques such as contouring, calculation of derivative products such as slope, aspect, various overlays of different derived grids, and direct examination of the DTM are common techniques used for DTM analysis (Engelkemeir and Khan, 2008), but did not prove to be as effective as hillshading for scarp identification, with the results being harder to interpret. Previous work (e.g., Ganas et al., 2005; Engelkemeir and Khan, 2008) found hillshading to be the most effective method for visualizing surface faults. Hillshading is controlled by both light source elevation and azimuth. Low sun elevation angles were noisy, primarily highlighting roads and creeks, whereas high angles resulted in less contrast. A medium angle, such as 45°, proved best for this study. With the regional N-S fault trend (cfr. **Figure 2**) an azimuth of 270° would highlight the scarps consistently with the regional trend in the DAD.

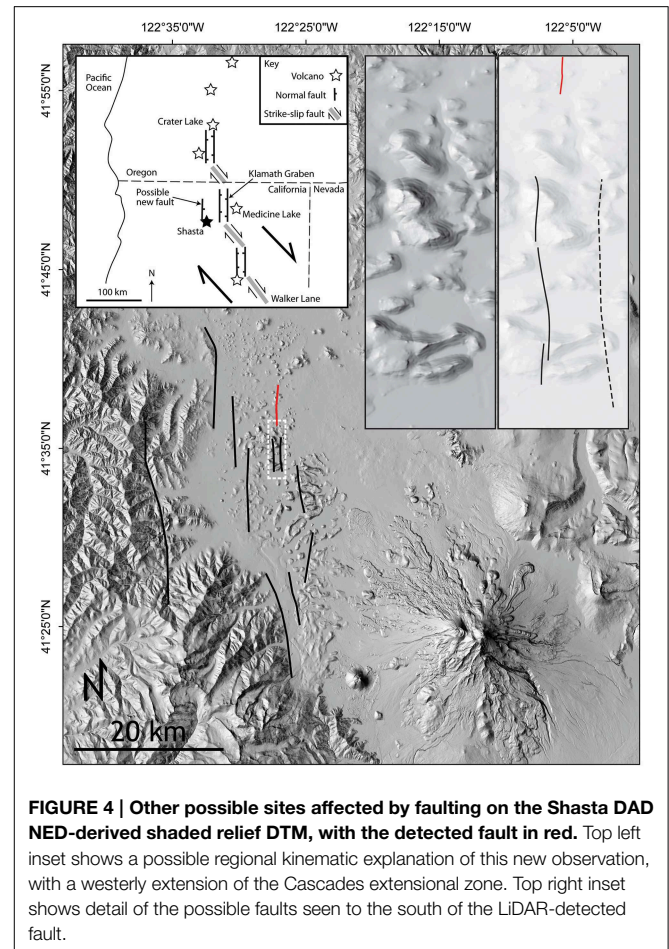
We made a field visit to the area for validation in December 2013. The hummocks are made of highly brecciated jig-saw cracked material with a breccia cover, typical of debris avalanche materials. Such granular deposits do not allow diagnostic structural features, such as fault planes or striations, to develop, but instead produce diffuse shear zones (e.g., van Wyk de Vries and Davis, 2015). In addition the granular nature of the rock does not permit development of clear fault scarps, leading to the subdued expression of the scarps that are hard to see in the field, and only really clear in the LiDAR data. More structural detail might be found on the lava outcrops, but these are also prefractured, and do not tend to preserve structural evidence, other than tension fractures. A full survey of the Shasta area, after a wider LiDAR survey would be an important and interesting further step, to analyze the different morphological expression of the faulting in different locations and lithologies.

## Results

Visual interpretation of the hillshaded LiDAR DTM revealed unexpectedly long fault-like scarps within the Shasta DAD.



Although digital maps published by the U.S. Geological Survey (<http://earthquake.usgs.gov/hazards/qfaults/map/>) and the California Geological Survey (Jennings and Bryant, 2010) do not show the presence of any fault in the Shasta DAD (cfr. **Figure 2**). A long N-S trend to lineament that cut the hummocks with characteristic fault surface break segmentation was identified (**Figure 3**). These features were not visible on other lower resolution DTMs (e.g., National Elevation Dataset, 10 m horizontal resolution), and the general N-S trend was located with hindsight. The hillshaded image provides a clear indication of the fault scarp (**Figure 3A**), whereas the scarp elevation contrast in the DTM and its first derivative (i.e., slope) product is noticeable but harder to observe (**Figure 3B**). The estimated minimum vertical displacement in the faulted region appears to be in the range of 3–10 m (**Figure 3E**).



## Discussion

The detection of a previously unmapped 2 km long lineament resembling a normal fault, with at least 3 m of apparent vertical displacement on the Shasta DAD is surprising and prompts the question of its origin: is it related to the debris avalanche emplacement or is it a deeper-seated tectonic fault? Hummocks are clearly cut by the fault scarp, which cuts across one hummock flank and up and down another, as well as traversing interhummock areas (**Figure 3**). This indicates that the fault escarpment developed well after the hummocks were stabilized.

The hummock distribution around the fault is scattered and does not show any strong preferential orientation. However, there is an apparent grouping of three hummocks along the fault trend (**Figure 3**). This could indicate that there was a pre-existing topographic feature that affected the debris avalanche motion in this zone, and thus indicate the presence of a low N-S oriented escarpment before DAD emplacement. A post-avalanche basaltic lava flow abuts the scarp, which had already developed. To the north of the observed scarp the lavas occur on both sides of the lineament and are also cut by it. This is observable in the field in a vertical outcrop of lava on the edge of a lake (**Figure 3**).

Based on these observations, we conclude that the fault is older than the landslide and had already produced a low topographic scarp. It may have had a slight influence on the debris avalanche path, as some hummocks are apparently aligned along it (**Figure 3**). The fault had probably developed before the lava flows were emplaced, but has continued to move after the deposit stabilized.

As this is the first fault identified in the Shasta basin it is important to consider its origin. On one hand, the fault could be related to gravitational loading of the Mt Shasta edifice on the basin (e.g., as described in van Wyk de Vries and Davis, 2015). The fault is located at ~30 km distance from the edifice summit, further than other known examples such as Etna and Merapi. However, this falls in the range of volcanic spreading related structural influence at other large edifices, such as Cameroon (Kervyn et al., 2014) and Haddington (Delcamp et al., 2008). The gentle topographic profile of Mt Shasta would tend to result in transtensional accommodation of loading at the base, with consequent far field translation of blocks (e.g., Delcamp et al., 2008). In addition, the volcano is constrained within the Shasta basin, restricting any spreading to the north or south, which would also lead to increased far field deformation as shown for Cameroon (Kervyn et al., 2014). The scale and expression of the faulting would be expected to increase toward the edifice. Instead, the fault trace is lost toward the volcano and no other neotectonic feature was detected that might link it to the edifice. We stress, however, that we do not have LiDAR data for a critical area around the volcano base, so we cannot exclude the presence of faulting nearer the cone. On the other hand, the inferred fault orientation is consistent with regional tectonics, and the margins of the Shasta basin also have steep segments with N-S orientation. The basin may be a half-graben with a major fault on the south-west side that has not yet been mapped. This could be a pull-apart structure and could be a westward extension of the Klamath Graben, that lies just east of Shasta at the termination of the Walker Lane strike-slip zone (cfr. Henry et al., 2007). In both cases the identified lineament would then be a minor fault, related to a larger, as yet unidentified structure.

Using the 10 m resolution National Elevation Dataset DTM we have identified some potential N-S alignments in the deposit and adjacent areas, which could either be similar faults or structures related to the debris avalanche emplacement (**Figure 4**). One particular site just to the south of the identified fault has a north-trending apparent alignment that appears to cut several hummocks and a flat area. This is strongly suggestive of a neotectonic fault and extends the structures closer to Shasta, adding to the possibility of a volcanic loading effect. Further LiDAR survey for confirmation is required to verify the fault and to further test this hypothesis. If tectonic in origin, the whole

set of possible structures identified would support the pull-apart hypothesis, with possible gravitational influence from loading by the Shasta edifice; such a combination would be analogous to that identified at Iriga (Philippines; Paguican et al., 2012). Volcanic loading and regional tectonics act in concert to create structures. Such far field volcano-tectonic deformation has been described for both extensional and strike-slip situations (e.g., van Wyk de Vries and Merle, 1996, 1998). In addition, if the surface rupture zone (i.e., the total surface length of all fault segments) was commensurate with surface faults known to be associated with >M 4.7 events (e.g., Anderson et al., 1996), seismic hazards in the Shasta region would be more significant than previously recognized.

A last remaining question is whether this fault could be related to volcanic activity at Shasta. There are large post-avalanche lava flows on the DAD, and the scar on Mt Shasta is infilled by subsequent eruptive material. It may be that the basal lavas are located on similar structures, as some eruption vents have the same north-south alignment. However, our LiDAR data strip is too localized to gauge this possibility.

## Conclusions

High-resolution LiDAR has been shown to be a highly effective tool for identification of a previously unmapped active fault in the 300 ka BP Mt Shasta DAD (**Figure 4**). No other tectonic feature was identified in the dataset. The result shows the potential of LiDAR and the methodology to detect faults obscured by DADs on volcano flanks. In particular, this fault was likely active before and after the debris avalanche, and most likely represents a regional structure related to a westerly continuation of the Klamath basin. Based on this preliminary work, seismic hazards in the Shasta region would be more significant than previously recognized. More LiDAR data and further detailed mapping of the region appears warranted in order to map the full extent of the rupture zone. In addition, the LiDAR strip used in this study (**Figure 2**) covers less than one twelfth of the Shasta DAD, and thus more faults may be yet hidden around Shasta.

## Acknowledgments

RT is funded by NSF grant EAR0940839 (VHub—Cyberinfrastructure for volcano eruption and hazards modeling and simulation). The National Center for Airborne Laser Mapping (NCALM) provided the LiDAR data to RT as seed grant 2013-08. We are thankful to Valerio Acocella, Luis Lara, and the three reviewers for providing thoughtful comments on earlier drafts of this manuscript.

## References

- Acocella, V., and Neri, M. (2005). Structural features of an active strike-slip fault on the sliding flank of Mt. Etna (Italy). *J. Struct. Geol.* 27, 343–355. doi: 10.1016/j.jsg.2004.07.006
- Anderson, J. G., Wesnousky, S. G., and Stirling, M. W. (1996). Earthquake size as function of fault slip rate. *Bull. Seismol. Soc. Am.* 86, 683–690.
- Arrowsmith, J. R., and Zielke, O. (2009). Tectonic geomorphology of the San Andreas Fault zone from high resolution topography: an example from the Cholame segment. *Geomorphology* 113, 70–81. doi: 10.1016/j.geomorph.2009.01.002
- Blakely, R. J., Christiansen, R. L., Guffanti, M., Wells, R. E., Donnelly-Nolan, J. M., Muffler, L. J. P., et al. (1997). Gravity anomalies, Quaternary vents, and Quaternary faults in the southern Cascade Range, Oregon and California: implications for arc and backarc evolution. *J. Geophys. Res.* 102, 22513–22527. doi: 10.1029/97JB01516
- Borgia, A., Burr, J., Montero, W., Morales, L. D., and Alvarado, G. E. (1990). Fault propagation folds induced by gravitational failure and slumping of the central Costa Rica Volcanic Range: implications for large terrestrial and Martian volcanic edifices. *J. Geophys. Res.* 95, 14357–14382. doi: 10.1029/JB095iB09p14357
- Crandell, D. R., Miller, C. D., Glicken, H. X., Christiansen, R. L., and Newhall, C. G. (1984). Catastrophic debris avalanche from ancestral Mount Shasta volcano, California. *Geology* 12, 143–146.
- Delcamp, A., van Wyk de Vries, B., and James, M. R. (2008). The influence of edifice slope and substrata on volcano spreading. *J. Volcanol. Geotherm. Res.* 177, 925–943. doi: 10.1016/j.jvolgeores.2008.07.014
- Egnew, S. (2005). Detection of fault scarps in Louisiana and south Texas using LiDAR data. *GSA Abstr. Progr.* 37, 36.
- Engelkemeir, R. M., and Khan, S. D. (2008). Lidar mapping of faults in Houston, Texas, USA. *Geosphere* 4, 170–182. doi: 10.1130/GES00096.1
- Faulds, J. E., Henry, C. D., and Hinz, N. H. (2005). Kinematics of the northern Walker Lane: an incipient transform fault along the Pacific-North American plate boundary. *Geology* 33, 505–508. doi: 10.1130/G21274.1
- Ganas, A., Pavlides, S., and Karastathis, V. (2005). DEM-based morphometry of range-front escarpments in Attica, central Greece, and its relation to fault slip rates. *Geomorphology* 65, 301–319. doi: 10.1016/j.geomorph.2004.09.006
- Guffanti, M., and Weaver, C. S. (1988). Distribution of late cenozoic volcanic vents in the cascade range: volcanic arc segmentation and regional tectonic considerations. *J. Geophys. Res.* 93, 6513–6529. doi: 10.1029/JB093iB06p06513
- Harding, D. J., and Berghoff, G. S. (2000). “Fault scarp detection beneath dense vegetation cover: airborne LiDAR mapping of the Seattle fault zone, Bainbridge Island, Washington State,” in *Proceedings of the ASPRS Annual Conference* (Washington, DC).
- Harper, G. D., and Wright, J. E. (1984). Middle to Late Jurassic tectonic evolution of the Klamath Mountains, California-Oregon. *Tectonics* 3, 759–772.
- Haugerud, R. A., Harding, D. J., Johnson, S. Y., Harless, J. L., Weaver, C. S., and Sherrod, B. L. (2003). High-resolution Lidar topography of the Puget Lowland, Washington—a bonanza for Earth science. *GSA Today* 13, 4–10. doi: 10.1130/1052-5173(2003)13<0004:HLTOTP>2.0.CO;2
- Henry, C. D., Faulds, J. E., and dePolo, C. M. (2007). Geometry and timing of strike-slip and normal faults in the northern Walker Lane, northwestern Nevada and northeastern California: strain partitioning or sequential extensional and strike-slip deformation? *GSA Special Papers* 434, 59–79. doi: 10.1130/2007.2434(04)
- Hilley, G. E., and Arrowsmith, J. R. (2008). Geomorphic response to uplift along the Dragon’s Back pressure ridge, Carrizo Plain, California. *Geology* 36, 367–370. doi: 10.1130/G24517A.1
- Hilley, G. E., DeLong, S., Prentice, C., Blisniuk, K., and Arrowsmith, J. R. (2010). Morphologic dating of fault scarps using airborne laser swath mapping (ALSM) data. *Geophys. Res. Lett.* 37, L04301. doi: 10.1029/2009gl042044
- Jennings, C. W., and Bryant, W. A. (2010). *Fault Activity Map of California*. California Geological Survey Geologic Data Map No. 6, map scale 1:750,000.
- Kervyn, M., van Wyk de Vries, B., Walter, T. R., Njome, M. S., Suh, C. E., and Ernst, G. G. J. (2014). Directional flank spreading at Mount Cameroon volcano: evidence from analogue modeling. *J. Geophys. Res.* 119, 7542–7563. doi: 10.1002/2014JB011330
- Kondo, H., Toda, S., Okumura, K., Takada, K., and Chiba, T. (2008). A fault scarp in an urban area identified by LiDAR survey: a case study on the Itoigawa–Shizuoka Tectonic Line, central Japan. *Geomorphology* 101, 731–739. doi: 10.1016/j.geomorph.2008.02.012
- Lin, Z., Kaneda, H., Mukoyama, S., Asada, N., and Chiba, T. (2013). Detection of subtle tectonic-geomorphic features in densely forested mountains by very high-resolution airborne LiDAR survey. *Geomorphology* 182, 104–115. doi: 10.1016/j.geomorph.2012.11.001
- Matsuda, T., Ota, Y., Ando, M., and Yonekura, N. (1978). Fault mechanism and recurrence time of major earthquakes in southern Kanto district, Japan, as deduced from coastal terrace data. *GSA Bull.* 89, 1610–1618.
- McGovern, P. J., Smith, J. R., Morgan, J. K., and Bulmer, M. H. (2004). Olympus Mons aureole deposits: new evidence for a flank failure origin. *J. Geophys. Res.* 109, E08008. doi: 10.1029/2004JE002258
- Morris, E. C. (1982). Aureole deposits of the Martian volcano Olympus Mons. *J. Geophys. Res.* 87, 1164–1178. doi: 10.1029/JB087iB02p01164
- Paguican, E. M. R., van Wyk de Vries, B., and Lagmay, A. M. F. (2012). Volcano-tectonic controls and emplacement kinematics of the Irga debris avalanches (Philippines). *Bull. Volcanol.* 74, 2067–2081. doi: 10.1007/s00445-012-0652-7
- Petrie, G., and Toth, C. K. (2009). “Airborne and spaceborne laser profilers and scanners,” in *Topographic Laser Ranging and Scanning: Principles and Processing*, eds J. Shan and C. K. Toth (Boca Raton, FL: CRC Press), 30–83.
- Pfeifer, N., and Mandlbürger, G. (2009). “LiDAR data filtering and DTM generation,” in *Topographic Laser Ranging and Scanning: Principles and Processing*, eds J. Shan and C. K. Toth (Boca Raton, FL: CRC Press), 308–331.
- Richards, J. P., and Villeneuve, M. (2001). The Llullaillaco volcano, northwest Argentina: construction by Pleistocene volcanism and destruction by sector collapse. *J. Volcanol. Geotherm. Res.* 105, 77–105. doi: 10.1016/S0377-0273(00)00245-6
- Schmidt, M. E., Grunder, A. L., and Rowe, M. C. (2008). Segmentation of the Cascade Arc as indicated by Sr and Nd isotopic variation among diverse primitive basalts. *Earth Planet. Sci. Lett.* 266, 166–181. doi: 10.1016/j.epsl.2007.11.013
- Shea, T., and van Wyk de Vries, B. (2008). Structural analysis and analogue modeling of the kinematics and dynamics of rockslide avalanches. *Geosphere* 4, 657–686. doi: 10.1130/GES00131.1
- Shea, T., van Wyk de Vries, B., and Pilato, M. (2008). Emplacement mechanisms of contrasting debris avalanches at Volcán Mombacho (Nicaragua), provided by structural and facies analysis. *Bull. Volcanol.* 70, 899–921. doi: 10.1007/s00445-007-0177-7
- Stumpf, A., Malet, J.-P., Kerle, N., Niethammer, U., and Rothmund, S. (2013). Image-based mapping of surface fissures for the investigation of landslide dynamics. *Geomorphology* 186, 12–27. doi: 10.1016/j.geomorph.2012.12.010
- van Wyk de Vries, B., and Davis, T. (2015). “Landslides, debris avalanches, and volcanic gravitational deformation,” in *Encyclopaedia of Volcanoes*, eds H. Sigurdsson, B. Houghton, S. McNutt, H. Rymer, and J. Stix (Amsterdam: Elsevier), 665–685.
- van Wyk de Vries, B., and Merle, O. (1996). The effect of volcanic constructs on rift fault patterns. *Geology* 24, 643–646.
- van Wyk de Vries, B., and Merle, O. (1998). Extension induced by volcanic loading in regional strike-slip zones. *Geology* 26, 983–986.
- van Wyk de Vries, B., Self, S., Francis, P. W., and Keszthelyi, L. (2001). A gravitational spreading origin for the Socompa debris avalanche. *J. Volcanol. Geotherm. Res.* 105, 225–247. doi: 10.1016/S0377-0273(00)00252-3
- Wadge, G., Francis, P. W., and Ramirez, C. F. (1995). The Socompa collapse and avalanche event. *J. Volcanol. Geotherm. Res.* 66, 309–336. doi: 10.1016/0377-0273(94)00083-S
- Walter, T. R., Wang, R., Zimmer, M., Grosser, H., Luhr, B., and Ratdomopurbo, A. (2007). Volcanic activity influenced by tectonic earthquakes: static and dynamic stress triggering at Mt. Merapi. *Geophys. Res. Lett.* 34, L05304. doi: 10.1029/2006gl028710
- Wehr, A. (2009). “LiDAR systems and calibration,” in *Topographic Laser Ranging and Scanning: Principles and Processing*, eds J. Shan and C. K. Toth (Boca Raton, FL: CRC Press), 129–171.

- Wieczorek, G. F., Harrison, R. W., Morgan, B. A., Weems, R. E., and Obermeier, S. F. (2004). Detection of faults and fault traces in the Shenandoah Valley, Virginia, using LiDAR imagery. *GSA Abstr. Progr.* 36, 120.
- Wooller, L., van Wyk de Vries, B., Murray, J. B., Rymer, H., and Meyer, S. (2004). Volcano spreading controlled by dipping substrata. *Geology* 32, 573–576. doi: 10.1130/G20472.1
- Zielke, O., Arrowsmith, J. R., Ludwig, L. G., and Akçiz, S. O. (2010). Slip in the 1857 and earlier large earthquakes along the Carrizo Plain, San Andreas Fault. *Science* 327, 1119–1122. doi: 10.1126/science.1182781

**Conflict of Interest Statement:** The authors declare that the research was conducted in the absence of any commercial or financial relationships that could be construed as a potential conflict of interest.

*Copyright © 2015 Tortini, van Wyk de Vries and Carn. This is an open-access article distributed under the terms of the Creative Commons Attribution License (CC BY). The use, distribution or reproduction in other forums is permitted, provided the original author(s) or licensor are credited and that the original publication in this journal is cited, in accordance with accepted academic practice. No use, distribution or reproduction is permitted which does not comply with these terms.*